Available online at www.sciencedirect.com
SCIENCE DIRECT
European Polymer Journal 42 (2006) 516–533
EUROPEAN POLYMER JOURNAL
www.elsevier.com/locate/europolj

Confinement effects on the crystallization and SSA thermal fractionation of the PE block within PE-*b*-PS diblock copolymers

A.T. Lorenzo [a], M.L. Arnal [a], A.J. Müller [a,*], A. Boschetti de Fierro [b], V. Abetz [b]

[a] *Grupo de Polímeros USB, Departamento de Ciencia de los Materiales, Universidad Simón Bolívar, Apartado 89000, Caracas 1080-A, Venezuela*
[b] *Institut für Polymerforschung, GKSS-Forschungszentrum Geesthacht GmbH, 21502 Geesthacht, Germany*

Received 8 July 2005; received in revised form 17 August 2005; accepted 6 September 2005
Available online 17 October 2005

Abstract

Well defined polyethylene-*b*-polystyrene (PE-*b*-PS) diblock copolymers have been synthesized by anionic polymerization in a wide composition range, keeping the length and the microstructure of the PE block constant. These copolymers provide a model system to study the confined crystallization of PE. A fractionated crystallization behavior (i.e., multiple exotherms are observed upon cooling from the melt) was observed for the PE block within block copolymers with 26% and 11% PE (i.e., $E_{26}S_{74}^{105}$ and $E_{11}S_{89}^{244}$ diblock copolymers, where the subscripts indicate the composition in wt% and the superscript the molecular weight in kg/mol). For confined PE, annealing is always observed when the material is self-nucleated. In the case of $E_{11}S_{89}^{244}$, most of the PE spheres crystallize at very large supercoolings, a behavior previously reported in the literature and associated with homogeneous nucleation. However, in our case, the peak crystallization temperature (i.e., $T_c = 46.6$ °C) is much lower (16 °C) than that reported for similar size PE nano-droplets but in diblock copolymer whose second block is chemically different to PS. We therefore conclude that the nature of the interphase between the two neighboring blocks may be responsible for such low temperature nucleation, since this T_c is still quite high with respect to the vitrification temperature of PE (in comparison with other polymers whose homogeneous nucleation temperature has been found close to T_g), a fact that could indicate that the homogeneous nucleation temperature has not been reached because surface (or interfacial) effects can dominate. Thermal fractionation takes advantage of the distribution of methyl sequence length in hydrogenated polybutadiene in order to produce by successive thermal annealing a distribution of lamellar thickness within each PE block. Such a distribution of thermal fractions is affected by confinement and therefore these experiments demonstrate the influence of morphological restrictions on the crystallization of the PE block within the PE-*b*-PS diblock copolymers. As the PE content in the copolymer decreases, topological confinement effects limit the size of the lamellar crystals that can be formed within the reduced dimensions of the microdomains (MD). By the use of the Gibbs-Thomson equation and the thermal fractionation results, a distribution of crystalline lamellar thickness within each MD was obtained and the orientation of the chains within the MD was deduced.

Keywords: Block copolymers; Confinement; SSA; Thermal fractionation; Crystallization

* Corresponding author. Tel./fax: +58 212 9063388.
E-mail address: amuller@usb.ve (A.J. Müller).

0014-3057/$ - see front matter © 2005 Elsevier Ltd. All rights reserved.
doi:10.1016/j.eurpolymj.2005.09.001

1. Introduction

Diblock copolymers present a neat way to produce controlled dispersions of isolated cylinders or spheres that serve as a model to study nucleation and crystallization of confined micro- or nano-domains. The crystallization of block copolymers with one or more crystallizable blocks is a subject that has attracted much recent attention [1–37]. The structure formation during crystallization from a microphase-separated melt is related to whether or not the self-assembly is disrupted by crystallization. The microdomain can change its shape (if crystallization overrides the phase separated morphology), or it can be maintained during crystallization (strong confinement). In block copolymers with a glassy amorphous component, crystallization may not be able to disturb the microphase structure in those cases where strong segregation between the components exists and vitrification of the amorphous block occurs at temperatures well above the crystallization temperature of the adjacent block. When a crystallizable block is subdivided into isolated microdomains (MDs), whose number is significantly greater than the number of usually active heterogeneities, the crystallization process occurs in several exotherms at discrete temperatures upon cooling from the melt, a process that has been termed fractionated crystallization phenomenon, and that could in some cases lead to exclusive homogeneous nucleation [3,10,12,15,16,18,21–23,25,29,32,35,36]. The fractionated crystallization process has been reported in diblock copolymers [3,12,15,16,18,21–23,38,39], polymer blends [41–50] and more recently in triblock terpolymers [2,3,10,24,25,27,35,36]. The common occurrence of the fractionated crystallization phenomenon for a wide range of diblock and triblock copolymers has been recently reviewed [3,21]. The self-nucleation technique can be useful to study confined crystallization and was first applied by DSC to polymers by Fillon et al. [51]. In a self-nucleation (SN) experiment, a polymer with an initial crystalline ''standard'' state is heated up to a given temperature, denoted self-nucleation temperature (T_s). If T_s is high enough to melt most of the polymer except for a certain amount of crystal fragments, recrystallization takes place upon subsequent cooling, using as nuclei those crystallographically ''ideal'' seeds which are left unmolten. When T_s is lower, partial melting is achieved and a large population of crystals is not melted and therefore anneals during heat treatment at T_s. Normally, three self-nucleation *Domains* can be ascribed to bulk crystallizable polymers depending on the applied T_s. In *Domain I* or ''complete melting Domain'', the crystallization temperature (T_c) upon cooling from T_s remains constant and no self-nucleation can be detected. *Domain II* or ''self-nucleation Domain'' occurs when heat treatment at T_s causes a shift in crystallization temperature (during subsequent cooling from T_s) to higher temperatures with decreasing self-nucleation temperature. Finally, in *Domain III* or ''self-nucleation and annealing Domain'', annealing and self-nucleation take place simultaneously [51]. In block copolymers, factors like the volumetric fraction and degree of segregation affect the type of confinement and therefore modify the self-nucleation behavior. In case of AB and ABC block copolymers, the absence of the exclusive self-nucleation domain (*Domain II*) has been observed in systems where the crystallizable component (i.e., polyethylene, PE, poly(ethylene oxide), PEO or poly(ε-caprolactone), PCL) is confined and isolated in nanometer scale length MDs like cylinders and spheres [3,21,25,27,35,52].

The successive self-nucleation/annealing technique (SSA) is essentially a thermal fractionation method that is based on the sequential application of self-nucleation and annealing steps to a polymer sample. After thermal conditioning, as explained in Section 2, a final DSC heating run reveals the distribution of melting points induced by the SSA treatment as a result of the heterogeneous nature of the chain structure of the polymer under analysis or of the topological restraining upon the crystallization process in block copolymers samples. The SSA technique has been reviewed recently [53].

In this work, we study the thermal behavior of the crystallizable block within polystyrene-*b*-polyethylene linear AB diblock copolymers whose PE block length is kept constant. Through a systematic variation of PS content in the copolymers, the confinement effect of the strongly segregated PS phase on the PE phase is studied. Furthermore, this work demonstrates the usefulness of the SSA technique to study confinement effects induced by a glassy PS block on the crystallization and melting process of the covalently bonded PE block.

2. Experimental

2.1. Synthesis

Solvents and monomers for anionic polymerization were purified according to common procedures

described elsewhere [1,24,54,55]. The synthesis of poly(1,4-butadiene)-block-polystyrene diblock copolymers (PB-*b*-PS) and poly(1,4-butadiene) (PB) homopolymer was accomplished by sequential anionic polymerization of butadiene and styrene in benzene at 60 °C for butadiene (3 h) and 40 °C for Styrene (5 h) using *sec*-BuLi as initiator. The reaction was terminated using isopropanol followed by precipitation in the same solvent. We will employ the notation: $A_xB_y^m$, where the subscript numbers denote the mass fraction in weight percent and the superscript gives the number-averaged molecular weight M_n in kg/mol of the entire block copolymer (see Table 1). The synthesis process for all the diblock copolymers was designed in order to obtain a PB block in the block copolymers with the same molecular weight and the same content of 1.2 units as in the PB homopolymer (see Table 1).

2.2. Hydrogenation

The polyethylene-*b*-polystyrene diblock copolymer (PE-*b*-PS) and PE homopolymer (PE) were obtained by hydrogenation of the corresponding precursors PB-*b*-PS and PB. Homogeneous catalytic hydrogenation was carried out in degassed toluene (1.5–2 wt% solution of the polymer) at 60 °C and 60 bar H_2 pressure for three days using a Wilkinson catalyst $(Ph_3P)_3Rh(I)Cl$ (Aldrich, 1 mol% with respect to the number of double bonds of the PB block). Under the employed conditions the PB block gets completely hydrogenated as revealed by ^1H NMR (Bruker AC 250 spectrometer, results not shown). Purification was accomplished by precipitation into isopropanol. Further purification was performed in order to remove residual Wilkinson catalyst by refluxing the homopolymer or block copolymer solution in toluene with a small amount of concentrated hydrochloric acid, again followed by precipitation into isopropanol.

Table 1
Characteristics of the samples employed

Original copolymers	M_n (kg/mol) butadiene block	% 1.2 units	$\overline{M}_w/\overline{M}_n$	Copolymers after hydrogenation
PB^{24}	24.4	11.0	1.01	PE^{25}
$B_{78}S_{22}^{41}$	31.0	12.6	1.02	$E_{79}S_{21}^{41}$
$B_{51}S_{49}^{51}$	26.4	11.3	1.04	$E_{53}S_{47}^{51}$
$B_{25}S_{75}^{105}$	26.4	11.3	1.05	$E_{26}S_{74}^{105}$
$B_{11}S_{89}^{244}$	27.6	11.3	1.02	$E_{11}S_{89}^{244}$

2.3. Differential scanning calorimetry (DSC)

The PE-*b*-PS diblock copolymers and the PE homopolymer were analyzed with a Perkin–Elmer Pyris 1 instrument calibrated with cyclohexane and indium under high purity nitrogen atmosphere. The DSC scans were obtained at 10 °C/min using a sample mass between 7 and 10 mg. All DSC cooling curves were recorded after the samples were held in the melt at 140 °C for 3 min in order to erase all previous thermal history. The crystallization and melting enthalpies values were normalized with respect to the PE fraction in the block copolymers. More complex thermal treatments, like self-nucleation (SN) and successive self-nucleation and annealing (SSA), were employed and are described below.

2.3.1. Self-nucleation experiments (SN)

The self-nucleation and annealing experiment using DSC was originally applied by Fillon et al. [51] to isotactic polypropylene (PP). These experiments involved the partial melting of a crystalline "standard" state followed by recrystallization using as nuclei the crystal fragments produced in the partial melting stage. The detailed procedure used here is described as follows:

(a) Erasure of any previous thermal history by heating the sample up to 140 °C for 3 min. This step erases all crystalline memory of the material as far as the dynamic experiments in the DSC are concerned. In other words, only temperature-resistant heterogeneous nuclei remain and upon subsequent cooling, the polymer will always crystallize at the same peak crystallization temperature (if the same cooling rates are used). The last observation suggests that the nucleation density remains constant under these conditions.
(b) Creation of a "standard" thermal history by cooling at a rate of 10 °C/min to 0 °C. This step insures that the crystallization of the polymer under investigation occurs under the same dynamic conditions.
(c) Heating at 10 °C/min up to a self-nucleation temperature, that shall be termed T_s from now on. The thermal conditioning at T_s is performed for 5 min. The distinction between the domains can be performed by careful observations of the cooling runs (step d) from T_s and the final heating runs (step e).

(d) DSC cooling scans from T_s at a rate of 10 °C/min, where the effects of the thermal treatment will be reflected on the crystallization of PE. If the polymer has been self-nucleated, a shift of the peak crystallization temperature to higher temperatures as compared to the standard cooling run (step b) is expected.
(e) DSC heating scans from 0 to 140 °C, where the effects of the entire thermal treatment will also be reflected in the melting of PE. For instance, if annealing took place at T_s, then a second, higher melting peak may be seen.

2.3.2. Successive self-nucleation and annealing experiments (SSA)

The SSA technique was developed by Müller et al. [53,56,57], and enhances the potential molecular fractionation that occurs during crystallization, while encouraging annealing of the unmelted crystals at each stage of the process, so that small effects can be magnified.

Experimentally, the steps "a" to "c" of the SN method described above were repeated as the first part of this experiment. Special care should be taken in choosing the first T_s temperature to be used in step "c". Ideally, the first T_s should be high enough to melt most of the polymer, but low enough to leave some crystal fragments that can act as nuclei but will not anneal during the time at that T_s.

The following steps were performed immediately after steps "a" to "c":

(d) Cooling from T_s: The sample was cooled at 10 °C/min from T_s to 0 °C. During this process, the initially molten fraction of the polymer at T_s will crystallize during cooling using the unmolten crystal fragments produced in step "c" as self-nuclei.
(e) Heating up to a new T_s: The sample was heated once again at 10 °C/min, but this time up to a T_s which was 5 °C lower than the previous one, and this temperature was held for 5 min. This means that the unmolten crystallites at this T_s will anneal, some of the melted species may isothermally crystallize (after being self-nucleated by the unmelted crystals) while the rest of the molten crystallizable chain segments will only crystallize during the subsequent cooling from T_s.
(f) Steps "d" and "e" are repeated at increasingly lower T_s. The differences in T_s were always kept constant at 5 °C. The number of repetitions can be chosen to cover the entire melting range of the sample with a "standard" thermal history or a shorter range.
(g) Final melting: The sample was heated at 10 °C/min from 0 °C to 140 °C and a multiple melting endotherm was obtained.

The SSA procedure was performed on the PE homopolymer choosing a T_s of 102 °C, as the ideal self-nucleation temperature, and the T_s temperatures were varied from 102 to 72 °C at 5 °C intervals for a total of seven self-nucleation/annealing steps. The same parameters were applied to all the diblock copolymer samples in order to maintain a standard thermal treatment based on the homopolymer.

2.4. Transmission electron microscopy (TEM)

The bulk morphology of the PB-*b*-PS and PE-*b*-PS diblock copolymers was examined by bright field TEM using a JEOL 1220 operated a 100 kV. Films (around 1 mm thick) were prepared by casting from a 3 wt% solution of the sample in toluene at 70 °C in order to avoid gelation upon solvent evaporation. After complete evaporation of the solvent (≈1 week), the films were kept at 150 °C (lower than a T_{ODT} of 230 °C reported for this block copolymer system [58] in copolymers with molecular weights between 11 and 90 kg/mol) for 15 h to improve the morphological segregation. In the case of the PE diblock, these samples were kept for 3 h at a crystallization temperature in order to allow the maximum crystallization of the PE block. Later, the films were slowly cooled down to room temperature. Thin sections were cut at −130 °C using a LEICA EMFCS ultramicrotome equipped with a diamond knife. Staining of the precursor diblock copolymer was accomplished by exposing thin sections to OsO_4 (preferential staining of the amorphous PB block). The PE-*b*-PS systems (hydrogenated copolymers) were stained by exposure to RuO_4 vapor for a short time (≈10 min). A good contrast between stained PS blocks (dark) and bright non-stained PE blocks was obtained.

From the $E_{11}S_{89}^{244}$ diblock copolymer micrographs, the average number and volume diameters (d_n and d_v) of the particle cross-sections were measured; at least 100 spheres were counted and measured. The number and volume average diameters were obtained using the following equations [59]:

$$d_n = \sum n_i d_i \Big/ \sum n_i, \quad (1)$$

$$d_v = \sum n_i d_i^4 \Big/ \sum n_i d_i^3, \quad (2)$$

where n_i is the number of spheres "i" of diameter d_i.

The volume fraction of the dispersed phase was calculated from the following relationship:

$$X_v = \left(\frac{X_p}{\rho_d}\right)\left[\frac{X_p}{\rho_d + (1 - X_p)/\rho_m}\right], \quad (3)$$

where X_p is the weight fraction of the minor phase and ρ_d is the dispersed phase density and ρ_m is the matrix density.

The average particle number per cm^3 was determined from:

$$Ni = X_v/(\pi/6d_n^3). \quad (4)$$

3. Results and discussion

3.1. Morphology

Fig. 1 shows representative micrographs of selected PB-*b*-PS and PE-*b*-PS diblock copolymers. A diversity of microdomains (MDs) morphologies can be generated in diblock copolymers (i.e., lamellae, cylinders, gyroids and spheres), depending on the volumetric fraction of the blocks and on the segregation strength of the system, determined by χN (where χ is the Flory–Huggins interaction parameter and N, the block copolymer total chain length) [1]. In a semicrystalline block copolymer, like PE-*b*-PS, two forces can drive structure formation: microphase separation between unlike blocks in the melt (strong segregation), which favors the formation of nanometer length scale MDs, and crystallization of one block, which favors the formation of alternating amorphous and crystalline layers. When the non-crystallizing block is glassy and the segregation strength is strong, the overall melt structure is retained: crystallization occurs within the MDs, leading to an "order within order", where the glassy matrix can affect the crystallization phenomena [1–3].

We have observed by TEM the morphology of the non-hydrogenated block copolymer precursors ($B_{78}S_{22}^{41}$, $B_{51}S_{49}^{51}$, $B_{25}S_{75}^{105}$, $B_{11}S_{89}^{244}$) and that of the hydrogenated ones ($E_{79}S_{21}^{41}$,$E_{53}S_{47}^{51}$, $E_{26}S_{74}^{105}$, $E_{11}S_{89}^{244}$). The micrographs in Fig. 1 show typical lamellar, cylindrical and spherical morphology of selected non-hydrogenated and hydrogenated diblock copolymers. It was demonstrated that PB and PE blocks form morphologies varying from a continuous matrix to spheres depending on the composition of the PB or PE block, as it was expected [1].

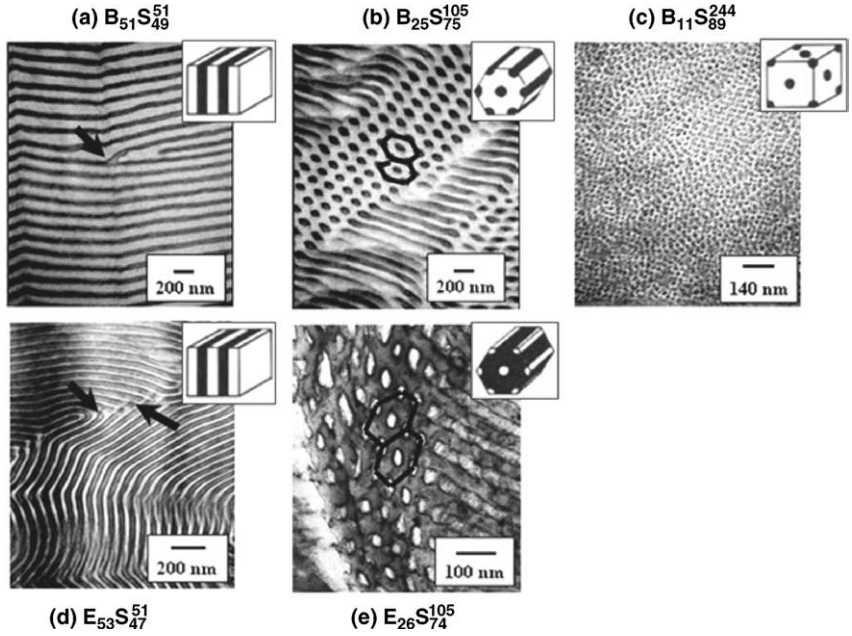

Fig. 1. TEM micrographs of the lamellae, cylinder and spheres forming diblock copolymers studied whose composition is indicated within. The PB-*b*-PS diblock copolymers were stained with OsO_4 (PS: gray: PB: dark) and the PE-*b*-PS diblock copolymers with RuO4 (PS: dark: PE: light gray).

In the case of the block copolymers with lamellar morphology shown in Fig. 1a and d ($B_{51}S_{49}^{51}$ and $E_{53}S_{47}^{51}$), the presence of alternating lamellae of each component can be clearly distinguished, as well as the existence of interconnected lamellae of the same block that can be considered as morphological defects (see arrows in the figures). For the PB or PE cylindrical morphology ($B_{25}S_{75}^{105}$ and $E_{26}S_{74}^{105}$, respectively) the transversal and longitudinal section can be observed in Fig. 1b and e, respectively. The hexagonal array of the cylinders is also clearly observed in the micrographs (Fig. 1b and e) selected for Fig. 1. If a comparison is made of the cylindrical morphology observed for $B_{25}S_{75}^{105}$ and $E_{26}S_{74}^{105}$, the PE cylinders appear somewhat deformed as compared to the regular PB cylinders. This is probably a consequence of crystallization, even though the PE crystallization occurs below the glass transition of the PS matrix in a rigidly confined fashion. When a semicrystalline block is confined within a diblock copolymer, Register and Loo have argued that three possibilities exist to accommodate the density change that occurs upon crystallization: existence of individual crystallized microdomains under significant hydrostatic tension, cavitation within the crystallizing domains and macroscopic contraction to accommodate the volume change [2]. From these, Loo et al. demonstrated in polyethylene-*b*-poly(vinylcyclohexane), PE-*b*-PVCH, copolymers that the third possibility is correct [18]. Even though the PVCH matrix is vitreous throughout crystallization, it can deform as necessary so that PE domains neither cavitate nor exist under great overall tension. This is in agreement with literature results that have shown evidences of deformation of confined core-shell cylinders [24,60].

For the $B_{78}S_{22}^{41}$ and $E_{79}S_{21}^{41}$ (micrographs not shown) a morphology of PS cylinders was found [15,16], while for the $B_{11}S_{89}^{244}$ (Fig. 1c) and $E_{11}S_{89}^{244}$, a disordered spheres morphology was observed with a mean mesophase diameter of 42 and 24 nm, respectively (see Table 2).

Due to the staining technique employed (long staining time) the boundary between the PE and the PS block, where the amorphous PE can be located, was remarkably stained resulting in a visible dark shade surrounding and delimiting the PE MDs in the hydrogenated block copolymers. This may lead to an underestimation in the measurements of the PE MDs dimension.

The hydrogenation process applied to the PB-*b*-PS precursors in order to obtain the PE-*b*-PS diblock copolymers did not affect the morphology as it has been reported in previous publications [24,61] for other block copolymers. Even as the PB block goes through a chemical change in its structure, the variation in the Flory–Huggins interaction parameter is very small (from $\chi_{B/S} = 4.71 \times 10^{-2}$ to $\chi_{E/S} = 5.51 \times 10^{-2}$ at room temperature [62]). Furthermore, the crystallization process does not seem to affect the morphology significantly after the hydrogenation process apart from the small deformation of the PE microdomains observed in the cylindrical case and a small reduction in MD size (see Fig. 1 and Table 2). These results confirm that both PB-*b*-PS and PE-*b*-PS diblock copolymers are in the strong segregation regime.

From experimental measurements on the PB-*b*-PS TEM micrographs and the application of the theory proposed for amorphous diblock copolymers by Abetz et al. [63], we obtained the size (''*l*'') and the periodicity value (''*d*'') of the MDs for the PB-*b*-PS block copolymers (see Table 2). From this table, it can be seen that the theory predicts in most cases in a satisfactory way the experimental dimensions obtained by TEM. Table 2 also lists

Table 2
Domain size ''*l*'' and spacing ''*d*'' of the PB-*b*-PS diblock copolymers as determined theoretically and by TEM

Copolymer	Theory		TEM		Morphology
	l (nm)	*d* (nm)	*l* (nm)	*d* (nm)	
$B_{51}S_{49}^{51}$	20 ± 1	85 ± 1	23 ± 4	88 ± 3	Lamellar
$B_{25}S_{75}^{105}$	26[b] ± 1	187[a] ± 1	25[b] ± 7	187[a] ± 8	PB cylinders
$B_{11}S_{89}^{244}$	15[b] ± 1	107[a] ± 2	21[b] ± 5	113[a] ± 16	PB spheres
$E_{53}S_{47}^{51}$	–	–	16 ± 3	62 ± 3	Lamellar
$E_{26}S_{74}^{105}$	–	–	21[b] ± 5	141[a] ± 8	PE cylinders
$E_{11}S_{89}^{244}$	–	–	12[b] ± 2	105[a] ± 13	PE spheres

[a] Interdomain distance.
[b] Radius of the microdomain.

the experimental variation of these parameters after the hydrogenation process of the PB-*b*-PS diblock copolymers. A decrease of both "*d*" and "*l*" is reported, a variation that can be a direct consequence of the crystallization process, although we have to take into consideration the possible error associated with MDs dimension measurement because of the presence of the dark shade boundary caused by staining.

We can conclude from this section that the morphology observed by TEM is that generally expected for this type of strongly segregated diblock copolymers and can be predicted by theory when the composition and χN values are taken into consideration [1,63].

3.2. Standard DSC results

DSC cooling scans from the melt and subsequent heating scans are presented in Fig. 2 for PE-*b*-PS diblock copolymers and for the neat hydrogenated PB. Table 3 lists all relevant transition temperatures and enthalpies extracted from Fig. 2.

One important aspect of the synthesis procedure employed here was to keep constant the molecular weight ($M_n \approx 26$ kg/mol) and the 1.2 units content (%1.2 units $\approx$ 11%) of the PE block within the diblock copolymers as well as in the PE homopolymer (see Table 1). In this way, we have eliminated the influence of these parameters in the thermal and morphological behavior of the diblock copolymers, allowing us to make more meaningful comparisons between the diblock copolymer system and the PE homopolymer.

The PE homopolymer exhibits a peak melting temperature (T_m) of 98.7 °C. In the block copolymers T_m does not change appreciably if the PE block forms a continuous or percolated phase ($E_{79}S_{21}^{41}$ and $E_{53}S_{47}^{51}$). When the morphological confinement increases ($E_{26}S_{74}^{105}$ and $E_{11}S_{89}^{244}$) the T_m value decreases markedly, for example, for the $E_{11}S_{89}^{244}$ copolymer the T_m is 85.2 °C. A decrease in the melting temperature (and in the enthalpy related to this process) indicates that the previous crystallization process was more difficult (i.e., it occurred at lower temperatures where thinner lamellar crystals that melt at lower temperatures are produced, see below) within each isolated MD when the confinement increased as a result of the increasing PS content.

The crystallization exotherm of PE^{25} displays a typical behavior that resembles that of ethylene/α-olefin copolymers, in view of its ethylene branch content produced by the 1.2 units in the precursor PB [53,64]. There is a main crystallization process that has been labeled "A" where most of the polymer crystallizes (at $T_c = 85.2$ °C as reported in

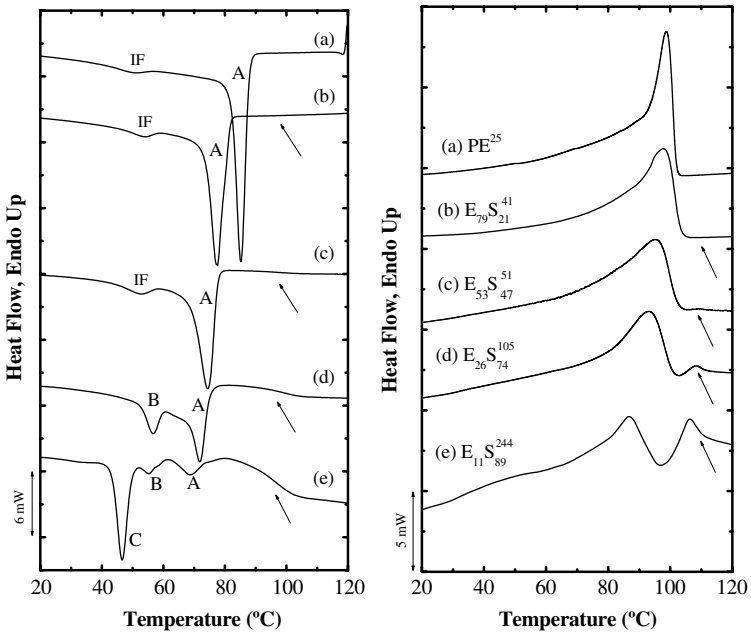

Fig. 2. Cooling (left) and heating (right) DSC scans (10 °C/min) for: (a) PE^{25}, (b) $E_{79}S_{21}^{41}$, (c) $E_{53}S_{47}^{51}$, (d) $E_{26}S_{74}^{105}$ and (e) $E_{11}S_{89}^{244}$. The curves were normalized in function to the PE content in the block copolymers. The arrows indicate the glass transition signal for the PS block in the copolymers.

Table 3
Thermal properties of the samples studied

	T_c (α), °C	T_c (β), °C	T_c (γ), °C	T_c (IF), °C	ΔH_c, J/g	$T_{m\,peak}$, °C	ΔH_f, J/g	X_c, %	$T_{g\,onset}$, °C	T_g, °C	T_m^0, °C[a]	Morphology
PE	85.2	–	–	51.3	−101	98.7	98	35	–	–	107.8	Bulk
$E_{79}S_{21}^{41}$	77.6	–	–	53.1	−74	98.0	76	26	101.9	105.1	107.2	PS cylinders
$E_{53}S_{47}^{51}$	74.4	–	–	52.8	−68	97.9	66	23	104.1	107.2	105.6	Lamellar
$E_{26}S_{74}^{105}$	71.8	56.5	–	–	−54	93.0	54	18	105.2	107.2	100.7	PE cylinders
$E_{11}S_{89}^{244}$	68.7	55.6	46.6	–	−36	85.2	45	15	106.9	107.4	95.6	PE spheres

[a] Values of T_m° were obtained by Hoffman–Weeks extrapolation after isothermal crystallization experiments.

Table 2). A much smaller exotherm appears around 50 °C. This small exotherm has been reported in a temperature range of 40–60 °C for branched polyethylenes in general and for linear low density polyethylene in particular. Such small secondary exotherms represent for bulk branch PE samples, the crystallization of short methylene sequence lengths (MSL) belonging to chains whose longer MSL crystallize at higher temperatures (in the exotherm labeled "A"), or in other words, the small exotherm at 40–60°C is due to intramolecular fractionation ("IF") during crystallization caused by the distribution of branches along the chains [64]. Therefore, this exotherm has been labeled "IF" to indicate its origin, its peak values are reported in Table 3.

In Fig. 2 we have labeled each important crystallization exotherm with "A", "B" and "C". In the case of PE[25], $E_{79}S_{21}^{41}$ and $E_{53}S_{47}^{51}$, the existence of a unique crystallization signal ("A"), apart from the small "IF" exotherms, is evidence that the crystallization process is due to heterogeneous nucleation from heterogeneities that we have arbitrarily termed "A". This is the typically observed behavior for commercial thermoplastics and for block copolymers if the crystallizable block forms a continuous phase (as a matrix or as a result of a percolation path). For the $E_{53}S_{47}^{51}$, the latter is possible only if: (a) the interconnection (or percolation) level in the lamellar morphology allows the spread of secondary nucleation through out the crystallizable component, (b) the number of MDs is very similar to the number of active heterogeneities present in an equivalent bulk sample of the crystallizable homopolymer, and (c) a combination of "a" and "b". The satisfaction of any of the above conditions will cause heterogeneous nucleation and therefore a classic self-nucleation behavior for the crystallizable block.

For $E_{26}S_{74}^{105}$ (PE cylinders in a PS matrix) and $E_{11}S_{89}^{244}$ (PE spheres in a PS matrix) diblock copolymers, multiple crystallization exotherms are observed. This is probably caused by a fractionated crystallization phenomenon that is produced by the existence of different types of nucleation events [3,21,40]. Each crystallization exotherm begins with a specific nucleation event (e.g., heterogeneous, superficial or homogeneous). Since different fractions of MDs could be isolated or percolated, the nucleation events may vary. Also the heterogeneity type present in different MDs fractions may also vary. The fractionated behavior of the crystallization process is due to the high MDs density (according to an estimation from TEM micrographs about $\sim 10^{12}$ and 10^{15} cm^{-3} for $E_{26}S_{74}^{105}$ and $E_{11}S_{89}^{244}$, respectively) in comparison with the heterogeneities concentration usually present in an equivalent bulk sample of the crystallizable polymer ($\sim 10^9$ cm^{-3} for the HDPE) [21]. Thus, fractionated crystallization will be present if there are MDs with different kinds of heterogeneities inside each population, the higher the heterogeneity nucleating efficiency the lower the supercooling needed by that specific fraction of MDs to crystallize. Nevertheless, the interconnection (or percolation) level in a fraction of the MDs could allow the spread of secondary nucleation through out the crystallizable component [21,23]. It must also be remembered that during hydrogenation a Wilkinson catalyst was used, and even though the sample was purified, catalyst particles that were not extracted could act as nucleating agent for those fractions that contained such heterogeneities. The lowest temperature crystallization signal could be originated from: (a) a weak nucleating heterogeneity, (b) superficial or interfacial nucleation events (due to the MDs interphase) or, (c) from homogeneous nucleation events [3,21].

Taking into consideration the possible explanations given above, for $E_{26}S_{74}^{105}$ the "A" crystallization signal is probably originated by the nucleation of "A" type heterogeneities (i.e., usually

available in bulk PE), but with some depression on the T_c value (in comparison with the high PE content copolymers or PE homopolymer) caused by the topological restrictions imposed by the PS matrix. The existence of a certain fraction of cylinders that contain such "A" type heterogeneity is probable, but also, if there are percolated cylinders, secondary nucleation can spread. Exotherm "B" could be caused by the presence of "B" type heterogeneities that are less active than "A", i.e., they require higher supercoolings to become active (for instance Wilkinson catalyst remaining particles). The superficial and the homogeneous nucleation events could be ruled out in the crystallization behavior of this block copolymer, especially for the "B" signal, because the $E_{11}S_{89}^{244}$ shows a lower crystallization exotherm (labeled "C"), as it will be analyzed next [21,40,42]. Finally, it must be noted that an overlap of exotherm "B" with an exotherm "IF" is possible in this case, however, exotherm "B" is more pronounced in relative terms (its enthalpic value is higher) in $E_{26}S_{74}^{105}$ than in block copolymers with higher PE content.

In a similar analysis, the $E_{11}S_{89}^{244}$ block copolymer exhibits three crystallization signals, a very clear example of a fractionated crystallization process [21,40–49]. Such a fractionated crystallization process with three exotherms in a block copolymer component that forms nano-spheres is uncommon, since the density of spheres is usually much higher than the number of heterogeneities available. However, in the present case, we also have another source of heterogeneities in the system, i.e., the Wilkinson catalyst employed. In the spherical morphology the weight fraction of PE is so small that percolation is highly unlikely and can be ruled out. Exotherm "A" is probably due to a nucleation event from "A" heterogeneities, like for the other copolymers mentioned above, in this case it is only a very small fraction of spheres that can crystallize in this high temperature range. The visible depression on the T_c value is caused by the confinement imposed by the surrounding glassy PS matrix. In an analogous way, exotherm "B" could be caused by a nucleation event from "B" heterogeneities (e.g., Wilkinson catalyst particles). The lowest crystallization temperature (exotherm "C" with a T_c of only 46.6 °C) can be ascribed to a superficial or homogeneous nucleation event (see below) due to the low T_c value found in comparison with reported values. In fact, as far as the authors are aware, this is the lowest value reported in the literature for PE crystallization, as shown in Table 4. Additionally, the crystallization enthalpy associated to this exotherm "C" is the highest in comparison with the enthalpies associated to the high temperature exotherms ("A" and "B") for $E_{11}S_{89}^{244}$, indicating that the relative fraction of material that crystallized at these lower temperatures is higher.

We have excluded in the above analysis the possibility that fractionated crystallization could be a result of a wide range of microdomain sizes (like in polyblends) since it is expected for anionically prepared diblock copolymers that a narrow distribution of microdomains sizes is obtained. For instance, in the case of PE spheres, TEM measurements (whose experimental error due to staining could be specially large in semicrystalline samples) yielded d_v/d_n values lower than 1.5 for the $E_{11}S_{89}^{244}$ diblock copolymer.

A relationship between the homogeneous nucleation temperature and the volume of the dispersed droplets is expected, since classical nucleation theory predicts that the probability of nucleation increases with the volume of the droplet. Such a relationship has been reported for some low molecular weight substances like water, alkanes and NaCl solutions, but the change in crystallization temperature reported has been very small, only 1–3 °C [65–68]. One polymer were a droplet size dependency of the homogeneous nucleation has been clearly established is poly(ethylene oxide), PEO. This was accomplished by Massa et al. [69,70] who employed their data on large (8–16 μm in diameter), isolated and clean droplets produced by dewetting a PEO film on an unfavorable PS surface and compared them with data by Röttele et al. [29] who studied by AFM the crystallization of PEO nano-spheres within a PB-*b*-PEO block copolymer. Crystallization data for a large difference in droplet volume is therefore available for PEO, i.e., a factor of approximately 10^9 difference in volume or 10^3 in diameter. Such a large difference in droplet size produced a maximum difference in the homogeneous crystallization temperature of 28 °C (minimum temperature −31 °C to a maximum temperature of −3 °C), an unusually large variation. This remarkable size dependence for PEO homogeneous nucleation temperature has been recently verified by Müller et al. [3] employing a wide range of data available in the literature that includes the already mentioned dewetted droplets [69,70], microemulsion droplets [71] and block copolymer spheres [3,16]. One way to distinguish between surface and bulk

Table 4
Lowest crystallization temperatures reported for the crystallization of materials that contain polyethylene as a confined dispersed phase

Material	PE content (wt%)	Branch content (%)	$T_{c\,peak}$ (°C)	Crystallization conditions	Morphology	Particle diameter	Reference
HDPE droplets/Igepal	–	–	85–87	Slow cooling	Droplets	<3 μm	[73]
HDPE droplets/ dibutyl phthalate	–	–	79–81	Slow cooling	Droplets	<3 μm	[73]
HDPE droplets/ dibutyl sebacate	–	–	80–82	Slow cooling	Droplets	<3 μm	[73]
HDPE droplets/ phenyl carbitol	–	–	82–84	Slow cooling	Droplets	<3 μm	[73]
LDPE/PS	20	–	53.5/61.5/ 70/100	2 °C/min	Droplets	–	[74]
HDPE droplets on glass treated with natural oil	–	–	74.8	1 °C/min	Droplets	–	[72]
HDPE droplets on glass treated with lanolin	–	–	79.0	1 °C/min	Droplets	–	[72]
HDPE droplets on glass treated with vacuum-evaporated carbon	–	–	127.0	1 °C/min	Droplets	–	[72]
HDPE droplets on glass treated with other surface agents	–	–	77.6/82.0/ 84.9/117.0	1 °C/min	Droplets	–	[72]
$E_{27}MB_{73}^{88}$	27	7	62		E cylinders	–	[7]
LLDPE/PS	10	–	105/73	10 °C/min	Droplets in blends	0.44–3.1 μm	[42]
	20	–	105/74	10 °C/min	Droplets in blends	0.48–3.2 μm	[42]
	30	–	102/72	10 °C/min	Droplets in blends	0.70–3.2 μm	[42]
	40	–	104/74	10 °C/min	Droplets in blends	0.90–4.4 μm	[42]
HDPE/PS	10	–	115.7/100.0/77.2	10 °C/min	Droplets in blends	0.14 μm	[43]
	20	–	115.2/108.5/ 76.8/68.5	10 °C/min	Droplets in blends	–	[43]
	30	–	115.7/77.5/ 66.6	10 °C/min	Droplets in blends	–	[43]
LLDPE/PS	10	–	67.3	10 °C/min	Droplets in blends	0.17 μm	[43]
	30	–	102.9/70.4/ 51.2	10 °C/min	Droplets in blends	0.23 μm	[43]
$E_{14}S_{86}^{54}$	14	8	66–70	Isothermal	E spheres	25 nm	[12]
$E_{18}V_{82}^{27}$	18	7	58	10 °C/min	E spheres	–	[18]
$E_{18}V_{82}^{31}$	18	7	63	10 °C/min	E cylinders	–	[18]
$E_{14}S_{86}^{64}$	14	8	62	10 °C/min	E spheres	–	[18]
$E_{14}S_{86}^{74}$	14	6	63	10 °C/min	E spheres	–	[18]
$E_{25}S_{75}^{70}$	25	7	63	10 °C/min	E cylinders	–	[18]
$E_{26}S_{74}^{105}$	26	11.3	71.8/56.5	10 °C/min	E cylinders	42 nm	This paper
$E_{11}S_{89}^{244}$	11	11.3	55.6/46.6	10 °C/min	E spheres	24 nm	This paper

HDPE: high density polyethylene; LDPE: low density polyethylene; E: ethylene; MB: poly(1,3 methyl-1-butene); LLDPE: linear low density polyethylene; PS: polystyrene; VCH: poly(vinyl cyclohexane); SEB: terpolymer of styrene-*ran*-ethylene-*ran*-butene; S: polystyrene.

homogeneous nucleation is to determine the scaling of the time constant, associated with the nucleation event (i.e., the particle diameter in the case of droplets) a technique that was successfully employed by Massa et al. [69].

Even though the size dependence of the true homogeneous nucleation temperature has been clearly established for some low molecular weight materials and for PEO, the situation is different for other polymers. For instance, in the case of

PCL, Müller et al. [3] have reviewed the literature and found no clear relationship between its homogeneous nucleation temperature and the size of the PCL MDs, even though a weak dependence has been reported by Nojima for one specific type of block copolymer [22]. Recently, Tol et al. have performed a detailed study of the fractionated crystallization of Nylon 6 dispersed as droplets in immiscible or compatibilized blends [48], they also found a dependence of the lowest crystallization temperature observed by DSC for Nylon droplets on the volume average droplet diameter (d_v). Temperature changes of between 6 and 8 °C were found depending on the blend system for droplets varying from 0.1 to 0.8 μm in d_v.

Barham et al. [72] studied the crystallization of sprayed HDPE droplets onto microscope glass slides by polarized optical microscopy. They reported that the lowest crystallization temperature for the droplets was dependent on the superficial treatment applied to the glass slide (between 74.8 and 127 °C, see Table 4). In view of these results, they proposed that the interface between the glass and the polymer droplet exhibited a weak nucleating effect on the HDPE. Tol et al. have also found surface nucleating effects in their Nylon 6 confined crystallization studies [48]. Arnal et al. [42,43] studied several PS/HDPE, PS/LLDPE (linear low-density polyethylene), and PS/ULDPE (ultra low-density polyethylene) blends. All the types of polyethylenes employed, when dispersed into droplets, exhibited fractionated crystallization exotherms, the lowest one was in the temperature range between 67 and 70 °C.

In the case of the diblock copolymers examined here, where polyethylene spheres are involved, we have found the lowest temperature ever reported for the crystallization upon cooling from the melt of PE droplets so far. However, we cannot ascribe this lower value to the fact that we have produced the smallest PE spheres, since this is not the case. Recently, Loo et al. [12] have studied the isothermal crystallization of the polyethylene block within a PE-*b*-SEB diblock copolymer constituted by hydrogenated polybutadiene (14.3 wt% PE) and an amorphous random terpolymer of styrene-*ran*-ethylene-*ran*-butene (SEB). The PE block crystallized within 25 nm spherical mesophases, and most spheres were supposed to have been homogeneously nucleated according to the authors because the number of MD was very large (2×10^{16} spheres/cm^3) and because the system exhibited first order crystallization kinetics. However, surface nucleation may also yield first order crystallization kinetics, this makes the distinction between surface and bulk homogeneous nucleation difficult [3,73–75,48]. Loo et al. [12] employed isothermal crystallization temperatures between 66 and 69 °C for the PE spheres within $E_{14}S_{86}^{54}$ and reported for similar materials (i.e., $E_{14}S_{86}^{64}$ and $E_{14}S_{86}^{74}$, see Table 4) peak crystallization temperatures upon cooling from the melt at 62–63 °C [23]. These last peak crystallization temperatures (that were also measured during cooling scans in the DSC at 10 °C/min) are approximately 16 °C higher than that found here for our $E_{11}S_{89}^{244}$ copolymer with similar size spherical MDs (see Table 4). We have taken into account all possible factors that can affect the nucleation temperature: the volume of the dispersed phase, the microstructure of the hydrogenated polybutadiene and the cooling rate (also whether isothermal or dynamic conditions apply, see Table 4). Having all these factors approximately constant, we still find a large difference in peak crystallization temperatures. The only important difference between the two types of PE spheres is that they are dispersed in different matrices, or in other words, the corresponding PE chains are covalently bonded to chemically different blocks, in our case the other block is PS (a glassy matrix at PE crystallization temperature) while in the work of Loo et al. it is PS-*ran*-PE-*ran*-PB (a rubbery matrix at PE crystallization temperature), both diblocks are in the strong segregation regime. We can only assume that it is this difference in the nature of the interphase between PE and the neighboring block that affects the nucleation.

The value of the T_g of PE has been under discussion for many years, however the two most frequently quoted values are approximately −30 and −120 °C [76,77]. This means that in the present case, our PE spheres are crystallizing at temperatures that are at least 70 °C above T_g. In a recent review, Müller et al. [3] analyzed the homogeneous nucleation temperatures in PE, establishing that the dynamic crystallization temperatures available in the literature for the PE as possibly associated with homogeneous nucleation are quite high in comparison with its T_g value (below at least −30 °C). This is not the case for other crystallizable polymers like PEO or PCL, which can exhibit crystallization temperatures if they are the minor components within block copolymers that are very close to their respective vitrification temperatures [10,21,78]. These low values for T_c suggest that in the PEO and the PCL case

true homogeneous nucleation temperatures have been obtained, since homogeneous nucleation should occur at the maximum possible supercooling (and nucleation events below T_g would be very unlikely).

Müller et al. [3] have argued that the true homogeneous nucleation temperature of PE may not have been found yet, since surface (or interphase) nucleation phenomena had not been entirely ruled out. The results of the present investigation support this view, since we have found lower crystallization temperatures for PE droplets than those reported in the literature, even though the PE spheres examined here have the same size range as those of Loo et al. [12]. A simple dependence of the homogeneous nucleation temperature on supercooling can be ruled out by comparing the maximum supercoolings that have been reported in the literature for the four most studied polymers in dispersed microphases, as shown in Table 5. It is clear from Table 5 that for PEO and PCL the lowest crystallization temperatures are very close to their respective T_g values (only 15–18 °C above T_g), while this is not the case for PE or even PP. Additionally, no correlation can be found between the lowest crystallization temperature and supercooling.

It could be that the reported low crystallization temperatures for PE droplets in the literature (and in this paper) are truly related to homogeneous nucleation, however, we have two problems with this interpretation: (1) So far, no clear demonstration that rules out superficial (or interfacial) nucleation in the case of PE has been provided in the literature, as far as the authors are aware (it must be noted, that for PEO, Massa and Dalnoki-Veress [70] have clearly demonstrated that volume nucleation is in place rather than surface nucleation), and; (2) No satisfactory explanation has been given as to why the homogeneous nucleation temperatures are much higher than T_g in the PE case as compared to other flexible polymers like PEO or PCL, when similar droplet volumes are considered (i.e., nano-spheres within block copolymers).

Coming back to Fig. 2, the glass transition of the PS block has been indicated with arrows for the PE-*b*-PS diblock copolymers and it is located around 107 °C. This transition can be better observed if the samples are quenched (at 60 °C/min) from the melt until 90 °C (i.e., at a temperature where the PE block has not been able to crystallize yet), and then heated at 20 °C/min. With this simple DSC procedure we can clearly distinguish the glass transition of the PS block for all diblock copolymers of this study (see Fig. 3). The observation of a similar value for the glass transition (see Table 3 and Fig. 3), for different PS compositions, is a clear evidence that the block copolymers are strongly segregated in the melt. The slight increase in T_g as PS content increases is ascribed to the increase in the molecular weight of the PS block.

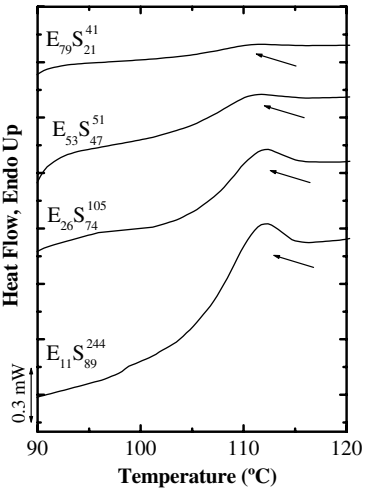

Fig. 3. Heating DSC scans (20 °C/min) for PE-*b*-PS diblock copolymers showing the glass transition signal in absence of PE block crystallization (see text). The arrows indicate the glass transition signal for the PS block in the copolymers.

Table 5
Comparison of interesting transition temperatures for four of the most studied polymers in dispersed form

Polymer	T_g (°C)[a]	Lowest reported T_c (°C)	T_m^0 (°C)[a]	$T_m^0 - T_c$ (°C)	$T_c - T_g$ (°C)	Reference
PEO	−67	−40.0	69.0	109.0	17.0	[21]
PCL	−64	−48.4	69.2	117.6	15.6	[21]
PP	−3	43.7	187.7	144.0	40.7	[45]
HDPE	−34	66.6	145.0	78.4	100.6	[43]
LLDPE	−34	51.2	145.0	93.8	85.2	[43]
PE^{25} within $E_{11}S_{89}^{244}$	−34	46.6	107.8	61.4	80.6	This paper

[a] From Ref. [78].

The DSC results analyzed in this section indicate that the crystallization of the PE block is affected by the covalent bond with the glassy PS block (especially in the $E_{79}S_{21}^{41}$ case) and by the topological restrictions given by the segregation in MDs like lamellae, cylinders and spheres (for $E_{53}S_{47}^{51}$, $E_{26}S_{74}^{105}$ and $E_{11}S_{89}^{244}$, respectively). The large number of MDs in the cylinder and the sphere morphology cases leads to fractionated crystallization. Self-nucleation studies can also be a valuable tool to study fractionated crystallization [3,16,21,25,27,35,42,47,51,52].

3.3. Self-nucleation studies

PE^{25}, $E_{79}S_{21}^{41}$ and $E_{53}S_{47}^{51}$ diblock copolymers were found to exhibit a "classic" self-nucleation behavior. This was expected for $E_{79}S_{21}^{41}$ since it is a diblock copolymer with a crystallizable block that forms a continuous matrix. In the case of $E_{53}S_{47}^{51}$, the classic self-nucleation behavior could be explained as a direct consequence of defects present in the lamellar morphology (see Section 3.1), in other words, the percolation level in this equilibrium morphology is high and this allows the spread of secondary nucleation through all the PE crystallizable material, in an analogous way as it happens in the $E_{79}S_{21}^{41}$ block copolymer and for the PE^{25} homopolymer.

For $E_{26}S_{74}^{105}$ a self-nucleation behavior that totally differs from the "classic" behavior was observed. The $E_{26}S_{74}^{105}$ diblock copolymer has two crystallization exotherms ("A" and "B") that exhibited two different self-nucleation behaviors. The "A" crystallization exotherm showed a "classic" behavior. The "B" exotherm did not exhibit the exclusive self-nucleation domain or *Domain II*; it exhibited a direct transition from *Domain I* to *Domain* III_{SA}, similar to the behavior exhibited by isolated MDs within block copolymers in previous publications [3,21,25,27,35,52].

In the case of $E_{11}S_{89}^{244}$, very atypical self-nucleation behavior was found for exotherms "B" and "C". The "A" exotherm of this copolymer showed the three classic domains of self-nucleation. For the very small "B" crystallization signal, a transition from *Domain I* to *Domain* III_{SA} was established for the self-nucleation behavior of this exotherm. In the case of the dominant "C" exotherm the self-nucleation was even more restricted, therefore, a transition from *Domain I* to *Domain* III_A was detected and finally, at lower temperatures, *Domain* III_{SA} was appreciated (results are not shown since they are similar to those previously shown in references [21,25,27,35,52]). In those cases where the injection of self-nuclei in every MD is most difficult in view of the very large number of MDs, *Domain III* has been observed to split into two domains [52], *Domain* III_A, where annealing without previous self-nucleation occurs and *Domain* III_{SA}, where self-nucleation and annealing are simultaneously observed. *Domain* III_{SA} would be the exact equivalent to the standard *Domain III* established by Fillon et al. [51].

3.4. Successive self-nucleation and annealing (SSA) studies

Fig. 4 shows a final heating DSC scan after SSA fractionation was performed to PE^{25} and to the block copolymer samples. The fractionated PE^{25} clearly shows a series of melting peaks that correspond to the melting of different mean lamellar thickness crystalline fractions that formed and annealed at each T_s temperature employed. The SSA fractionated PE^{25} final DSC heating scan shows the effects of the accumulation of 7 self-nucleation and annealing steps using T_s temperatures from 102 to 72 °C every 5 °C. Since 102 °C does not cause any annealing because it is a T_s temperature within *Domain II*, only 6 steps were able to produce annealing. The melting trace of PE^{25} after SSA

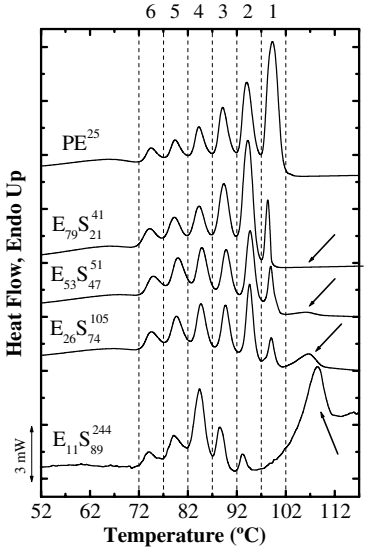

Fig. 4. DSC heating scans at 10 °C/min for the PE homopolymer and the PE-*b*-PS diblock copolymers after the SSA thermal treatment. The curves were normalized in function to the PE content in the block copolymer. The arrows indicate the glass transition signal for the PS block in the copolymers.

shows the melting of 6 fractions in Fig. 4, illustrating the capability of the technique to induce thermal fractionation in view of the monomodal and broad short chain branching (SCB) distribution of the PE^{25} evaluated. The SCB distribution in PE^{25} is totally random for the synthesis method used here, and this explains the monomodal distribution of melting peaks observed [53].

Fig. 4 also contains final heating scans for four PE-*b*-PS diblock copolymers. Even in the $E_{79}S_{21}^{41}$ diblock copolymer, whose morphology is a PE matrix with glassy polystyrene cylinders, the distribution of lamellar thickness obtained after SSA fractionation is different from that of PE^{25}. Fig. 4 shows how fraction number 1, the highest temperature fraction, is depleted in the $E_{79}S_{21}^{41}$ diblock copolymer (as compared to PE^{25}) and now the fraction with the largest area is number 2. This is caused by the difficulties experienced by the *PE* chains when they have one end covalently bound to a glassy *PS* block and they are trying to crystallize. Therefore, they can only form a small quantity of the largest lamellae that require the longest methylene sequence length (MSL) as compared to neat PE^{25}, where the chains have less diffusion problems to form the thickest lamellae.

As it was stated in the experimental part, the PE block within PE-*b*-PS diblock copolymers is very similar in M_w and in the content of 1.2 units to the PE homopolymer. Therefore, in this case all the differences that may be encountered in the thermal fractionation accomplished by SSA will be due to the morphological confinement on the PE block crystallization and not to differences in SCB content of the samples.

In Fig. 4, fraction named "1" (the one annealed at $T_s = 97$ °C) decreases in area as the PS content increases in the copolymer, until it totally disappears for the $E_{11}S_{89}^{244}$ copolymer. This phenomenon can be observed in a similar way for the second and third fractions (annealed at 92 and 87 °C, respectively). In general, a decrease in the high temperature melting peak areas and an increase in the low temperature melting peak areas are observed as the composition (PS content) varies in the copolymer. Therefore, the SSA method allows the qualitative observation of the topological chain restrictions associated with the crystallization of the PE block as the morphology changes from a PE matrix ($E_{79}S_{21}^{41}$), to PE lamellae ($E_{53}S_{47}^{51}$), PE cylinders ($E_{26}S_{74}^{105}$) and finally to PE spheres ($E_{11}S_{89}^{244}$) within the diblock copolymers and in comparison to the PE^{25} sample. The trends of the relative

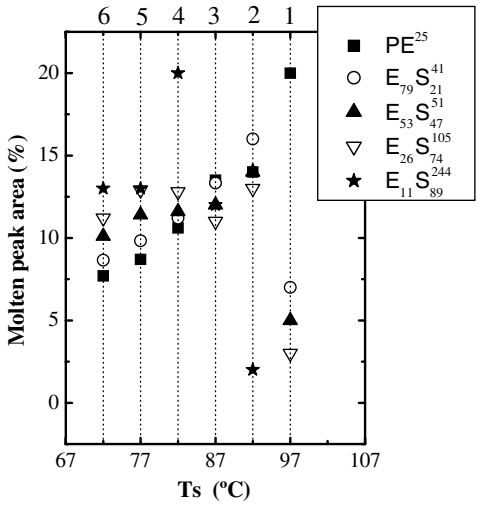

Fig. 5. % Melting area at each T_s for the homopolymer and the PE-*b*-PS diblock copolymers.

amounts of crystal populations with different melting temperatures can be seen in Fig. 5.

The influence of copolymer composition in the SSA results of Fig. 4 is very interesting. The copolymer that can form the largest amount of thicker lamellae is $E_{79}S_{21}^{41}$ since this is the copolymer with the highest PE content. Therefore, the PE chains will be less constrained to diffuse and produce thicker lamellae during the annealing process than $E_{11}S_{89}^{244}$ copolymer, in which the PE proportion is the lowest. For instance, for the $E_{11}S_{89}^{244}$ the most abundant fraction of lamellae are the ones that were originated at a T_s of 82 °C (fraction number 4) while in the PE^{25} this fraction was only the fourth most important and much less abundant, as judged by the molten peak area of each T_s value presented in Fig. 5. Since no change in the distribution of SCB is present in the PE phase for all samples, all changes in the distribution of melting points (or lamellar thickness) must be accounted for by morphological restrictions of the vitreous PS matrix on the PE domains.

3.4.1. Determination of mean lamellar thickness distributions by SSA

The final heating run after an SSA treatment exhibits a series of melting peaks that correspond to the number of SSA cycles where annealing was promoted. The differential area under such fusion curve can be related to the weight proportion of material that melts within the temperature interval considered. The Thomson–Gibbs equation [79] can

then be used to establish a correlation between temperature and lamellar thickness:

$$l = \frac{2 \cdot \sigma \cdot T_m^0 \cdot \Delta z}{\Delta h \cdot (T_m^0 - T_m)}. \quad (5)$$

We have employed the above equation using the values proposed recently by Cho et al. [79]: lamellar surface free energy ($\sigma = 5.0$ kJ mol^{-1}), enthalpy of fusion per C_2H_4-group ($\Delta h = 8.2$ kJ mol^{-1}), length of a C_2H_4-unit in the chain direction ($\Delta z = 0.254$ nm). The equilibrium melting temperature (T_m^0) was calculated from Hoffman–Weeks plots constructed with data obtained by isothermal crystallization of each system evaluated.

The values of mean lamellar thickness obtained in this work from the Thomson–Gibbs equation after the SSA treatment will only give a qualitative indication of the mean lamellar thickness distribution that can be useful for comparison purposes, especially since they can be quickly obtained via DSC measurements. A more rigorous determination of the lamellar thickness distribution could be obtained by Raman spectroscopy or other independent methods. The data obtained by DSC was used to calculate the lamellar thickness distribution, as presented in Fig. 6 [53,57]. It can be noticed that the peaks corresponding to thicker lamellae are broader than those of thinner lamellae. This is a consequence of the mathematical simplicity of Thomson–Gibbs equation in predicting smaller lamellar thickness changes with major temperature changes [53,80]. The effect of the covalently bonded PS block is clearly visible in the distribution of lamellar thickness of the block copolymers. The topological constraints imposed by the PS block produce a decrease in the amount of thicker lamellar as the PS content increases (see Fig. 6).

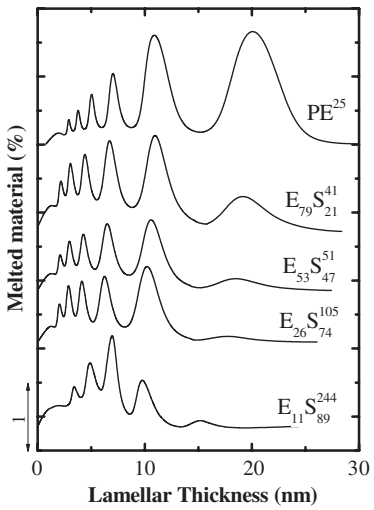

Fig. 6. Derived lamellar thickness distribution for PE^{25} and the PE-*b*-PS block copolymers using the SSA data and the Thomson–Gibbs equation.

Another important factor to take into consideration is that the values of lamellar thickness predicted by Eq. (5) are highly dependent on the value of T_m^0 that is used for the calculations. For instance, if the value of T_m^0 of linear PE is employed (i.e., 141–145 °C) the lamellar thickness values obtained will be lower than those reported in Fig. 6 by almost a factor of 6. In the case of Fig. 6 we have employed the T_m^0 values experimentally obtained for the PE and the PE block in the block copolymers samples [81].

In spite of all the above considerations on the limitations of the quantitative values of lamellar thicknesses, Fig. 6 illustrates the effect of morphological confinement on the crystalline lamellar sizes obtained and the values are consistent with the MD sizes reported in Table 2, in the sense that the lamellar thicknesses are always lower than the MDs relevant dimensions.

Fig. 7 shows a schematic diagram of how the crystallites could accommodate inside the microdomains present in the lamellar, cylinders and spheres forming diblock copolymers. In the lamellar case, since the thickness of the PE block lamellae is 16 nm (see Fig. 7 and Table 2), the only way that the thickest PE crystal population of $l = 21$ nm (according to Fig. 6) can fit within the MD is by having a chain orientation parallel to the MD interphase. This result is consistent with the literature since several authors agree that the most common crystal orientation for strongly segregated block copolymers is the one where chain folding is parallel to the diblock interphase, as drawn schematically in Fig. 7 [5,12,82].

When the MDs are cylinders, Loo et al. [83] found that chain folding was perpendicular to the cylindrical interphase in diblock copolymers of ethylene and vinylcyclohexane (in strong segregation regime), in the case of our PE-*b*-PS diblock copolymer we can apply this hypothesis due to the strong segregation observed for these copolymers, and again the MD size (cylinder diameter is approximately 42 nm, see Table 2 and Fig. 7) and the derived maximum crystal thickness (approximately 19 nm, see Figs. 6 and 7) are consistent. Finally, in the spheres forming case, the confinement upon

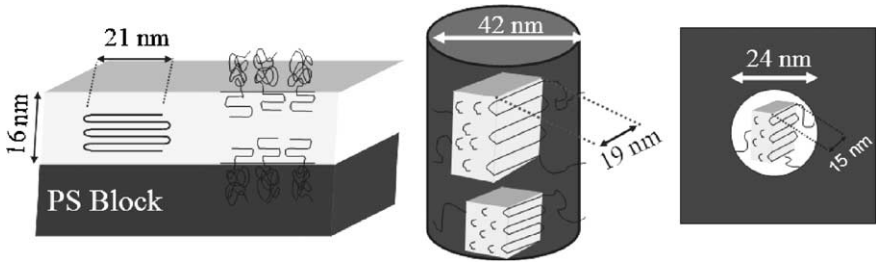

Fig. 7. Schematic of crystal orientation of the PE block in the lamellar (left), cylinders (middle) and spheres (right) forming diblock copolymers.

the PE block is three dimensional, the largest PE crystals (which in any case are the least abundant population) according to Fig. 6 have mean l values of approximately 15 nm while the sphere diameters (Table 2) are approximately 24 nm, so they could also fit within the MDs.

In a related work, Röttele et al. [29] have studied the thermodynamic properties of PEO spheres formed by the PEO block within a PB-*b*-PEO block copolymer. The spheres were homogeneously nucleated and therefore crystallized only at very large supercoolings, the resulting crystals were imperfect and showed significant reorganization during heating. They found that the PEO spheres displayed a broad melting range that was attributed to the superposition of the sharp first order transitions of the individual crystals, that take place at different temperatures corresponding to a multitude of possible metastable states. In the case of our SSA results, the self-nucleation and annealing process drives each fraction to the maximum stability that allows the particular MSL within the chain assembly.

4. Conclusions

The crystallization of the PE block has been shown to be influenced by the glassy PS block. Confinement effects and topological restrictions on the PE block increase as the PS content in the copolymers increases causing a decrease in both the crystallization and melting temperature of the PE block crystals. When the PE is confined to cylinders or spheres a fractionated crystallization phenomenon is induced by the excess MD density as compared to the available number density of nucleating heterogeneities.

In the case of $E_{11}S_{89}^{244}$, most of the PE spheres crystallize in one of the three exotherms encountered upon cooling from the melt, whose peak temperature (i.e., $T_c = 46.6$ °C) is the lowest temperature ever reported for PE droplet crystallization, a temperature that could be probably associated with surface or homogeneous nucleation. This crystallization temperature (i.e., $T_c = 46.6$ °C) is much lower (16 °C) than that reported for similar size PE nano-droplets but in diblock copolymer whose second block is chemically different to PS. We therefore conclude that the nature of the interphase between the two neighboring blocks may be responsible for such low temperature nucleation, since this T_c is still quite high with respect to the vitrification temperature of PE (in comparison with other polymers whose homogeneous nucleation temperature has been found close to T_g), a fact that could indicate that the homogeneous nucleation temperature has not been reached because surface (or interfacial) effects can dominate.

When the PE block forms a continuous or percolated phase (PE^{25}, $E_{78}S_{22}^{41}$ and $E_{53}S_{47}^{51}$), a "classic" self-nucleation behavior (i.e., three domains) was observed. When the PE block is dispersed as MDs and a fractionated crystallization was detected ($E_{26}S_{74}^{105}$ and $E_{11}S_{89}^{244}$), the fraction of crystals formed at higher temperatures exhibits a "classic" self-nucleation behavior, and those crystals that crystallize at the largest supercooling (lower exotherms) can only be self-nucleated at temperatures where the *Domain III* has already started and hence the *Domain II* disappears for this fraction of material.

Finally, SSA thermal fractionation experiments have shown the influence of morphological restrictions on the crystallization of the PE block within the PE-*b*-PS diblock copolymers. As the PE content in the copolymer decreased, topological confinement effects limited the size of the lamellar crystals that formed within the reduced dimensions of the microdomains (MD). A distribution of crystalline lamellar thickness within each MD was successfully obtained from the SSA results and the orientation of the chains within the MD was deduced.

Acknowledgments

Synthesis of the polymers was carried out at the University of Bayreuth. ATL and AB acknowledge financial support by Deutsche Forschungsgemeinschaft (SFB 481) during their time in Bayreuth. Further supports were given by Fonds der chemischen Industrie. The USB team acknowledges financial support from Fonacit through grant G97-000594 and the help of Mr. Edgar Cañizales in obtaining some of the TEM images.

References

[1] Hamley IW. The physics of block copolymers. Oxford: Oxford University Press; 1998.
[2] Loo YL, Register RA. Crystallisation within block copolymers mesophases. In: Loo Hamley IW, editor. New York: John Wiley & Sons; 2004.
[3] Müller AJ, Balsamo V, Arnal ML. Advances in polymer science, in press.
[4] Nojima S, Kato K, Yamamoto S, Ashida T. Macromolecules 1992;25:2237.
[5] Hamley IW, Fairclough JPA, Terrill NJ, Ryan AJ, Lipic PM, Bates FS, et al. Macromolecules 1996;29:8835.
[6] Ryan AJ, Fairclough JPA, Hamley IW, Mai SM, Booth C. Macromolecules 1997;30:1723.
[7] Quiram DJ, Register RA, Marchand GR. Macromolecules 1997;30:4551.
[8] Quiram DJ, Register RA, Marchand GR, Ryan AJ. Macromolecules 1997;30:8338.
[9] Floudas G, Reiter G, Lambert O, Dumas P. Macromolecules 1998;31:7279.
[10] Balsamo V, Müller AJ, Gyldenfeldt FV, Stadler R. Macromol Chem Phys 1998;199:1063.
[11] Balsamo V, Müller AJ, Stadler R. Macromolecules 1998;31:7756.
[12] Loo YL, Register RA, Ryan AJ. Phys Rev Lett 2000;84:4120.
[13] Zhu L, Cheng SZD, Calhoun BH, Ge Q, Quirk RP, Thomas EL, et al. Polymer 2001;42:5829.
[14] Zhu L, Mimnaugh BR, Ge Q, Quirk RP, Cheng SZD, Thomas EL, et al. Polymer 2001;42:9121.
[15] Reiter G, Castelein G, Sommer JU, Röttele A, Thurn-Albrecht T. Phys Rev Lett 2001;87:226101.
[16] Chen HL, Wu JC, Lin TL, Lin JS. Macromolecules 2001;34:2001.
[17] Hong S, MacKnight WJ, Russell TP, Gido SP. Macromolecules 2001;34:2398.
[18] Loo YL, Register RA, Ryan AJ, Dee GT. Macromolecules 2001;34:8968.
[19] Shiomi T, Tsukada H, Takeshita H, Takenaka K, Tezuka Y. Polymer 2001;42:4997.
[20] Shiomi T, Takeshita H, Kawaguchi H, Nagai M, Takenaka M, Miya M. Macromolecules 2002;35:8056.
[21] Müller AJ, Balsamo V, Arnal ML, Jakob T, Schmalz H, Abetz V. Macromolecules 2002;35:3048.
[22] Nojima S, Toei M, Hara S, Tanimoto S, Sasaki S. Polymer 2002;43:4087.
[23] Loo YL, Register RA, Ryan AJ. Macromolecules 2002;35:2365.
[24] Schmalz H, Knoll A, Muller AJ, Abetz V. Macromolecules 2002;35:10004.
[25] Muller AJ, Arnal ML, López-Carrasquero F. Macromol Symp 2002;183:199.
[26] Albuerne J, Márquez L, Muller AJ, Raquez JM, Degée Ph, Dubois Ph, et al. Macromolecules 2003;36:1633.
[27] Schmalz H, Müller AJ, Abetz V. Macromol Chem Phys 2003;204:111.
[28] Ueda M, Sakurai K, Okamoto S, Lohse D, MacKnight WJ, Shinkai S, et al. Polymer 2003;44:6995.
[29] Röttele A, Thurn-Albrecht T, Sommer JU, Reiter G. Macromolecules 2003;36:1257.
[30] Reiter G. J Polym Sci Part B: Polym Phys 2003;41:1869.
[31] Sun L, Zhu L, Ge Q, Quirk RP, Xue C, Cheng SZD, et al. Polymer 2004;45:2931.
[32] Xu JT, Ryan AJ, Mai SM, Yuan JJ, Cheng SY. J Macromol Sci B 2004;43:685.
[33] Sun L, Liu Y, Zhu L, Hsiao BS, Avila-Orta CA. Polymer 2004;45:8181.
[34] Nojima S, Akutsu Y, Washino A, Tanimoto S. Polymer 2004;45:7317.
[35] Arnal ML, López-Carrasquero F, Laredo E, Müller AJ. Eur Polym J 2004;40:1461.
[36] Balsamo V, Urdaneta N, Pérez L, Carrizales P, Abetz V, Muller AJ. Eur Polym J 2004;40:1033.
[37] Müller AJ, Albuerne J, Marquez L, Raquez JM, Degée P, Dubois P, et al. Faraday Discuss 2005;128:231.
[38] Lotz B, Kovacs AJ. Polym Prep (ACS, Polym Chem Div) 1969;10:820.
[39] O'Malley JJ. J Polym Sci Polym Symp 1977;60:151.
[40] Frensch H, Harnischfeger P, Jungnickel BJ. Fractionated crystallization in incompatible polymer blends. In: Utracky LA, Weiss RA, editors. Multiphase polymers: blends and ionomers. ACS Symp Ser.
[41] Santana OO, Müller AJ. Polym Bull 1994;32:471.
[42] Arnal ML, Matos ME, Morales RA, Santana OO, Müller AJ. Macromol Chem Phys 1998;199:2275.
[43] Arnal ML, Müller AJ. Macromol Chem Phys 1999;200:2559.
[44] Everaert V, Groeninckx G, Aerts L. Polymer 2000;41:1409.
[45] Arnal ML, Müller AJ, Maiti P, Hikosaka M. Macromol Chem Phys 2000;201:2493.
[46] Groeninckx G, Vanneste M, Everaert V. Crystallization, morphological structure and melting of polymer blends. In: Utracki LA, editor. Polymer blends handbook. Dordrecht: Kluwer Academic Publishers; 2002.
[47] Tol RT, Mathot VBF, Groeninckx G. Polymer 2005;46:369.
[48] Tol RT, Mathot VBF, Groeninckx G. Polymer 2005;46:383.
[49] Tol RT, Mathot VBF, Groeninckx G. Polymer 2005;46:2955.
[50] Tol RT, Mathot VBF, Reynaers H, Goderis B, Groeninckx G. Polymer 2005;46:2966.
[51] Fillon B, Wittman JC, Lotz B, Thierry A. J Polym Sci B 1993;31:1383.
[52] Balsamo V, Paolini Y, Ronca G, Müller AJ. Macromol Chem Phys 2000;201:2711.
[53] Müller AJ, Arnal ML. Prog Polym Sci 2005;30:559.
[54] Schmalz H, Abetz V, Lange R, Soliman M. Macromolecules 1998;31:7179.
[55] Schmalz H, Böker A, Lange R, Krausch G, Abetz V. Macromolecules 2001;34:8720.

[56] Müller AJ, Hernández ZH, Arnal ML, Sánchez JJ. Polym Bull 1997;39:465.
[57] Arnal ML, Balsamo V, Ronca G, Sánchez A, Müller AJ, Cañizales E, et al. J Therm Anal Calor 2000;59:451.
[58] Cohen RE, Cheng PL, Douzinas K, Kofinas P, Berney CV. Macromolecules 1990;23:324.
[59] Chandrasekar S. Rev Mod Phys 1943;15:1.
[60] Balsamo V, Von Gyldenfeldt F, Stadler R. Macromolecules 1999;32:1226.
[61] Stadler R, Auschra C, Beckmann J, Krappe U, Voigt-Martin I, Leibler I. Macromolecules 1995;28:3080.
[62] Mark JE. Physical properties of polymers handbook. New York: American Institute of Physics; 1996.
[63] Abetz V, Stadler R, Leibler L. Polym Bull 1996;37:135.
[64] Mathot VBF. Calorimetry and thermal analysis of polymers. New York: Hanser Publishers; 1994.
[65] Talsma H, van Steenbergen MJ, Crommelin DJA. Cryobiology 1992;29:80.
[66] Montenegro R, Landfester K. Langmuir 2003;19:5996.
[67] Janssen AH, Talsma H, van Steenbergen MJ, de Jong KP. Langmuir 2004;20:41.
[68] Montenegro R, Antonietti M, Mastai Y, Landfester K. J Phys Chem B 2003;107:5088.
[69] Massa MV, Carvalho JL, Dalnoki-Veress K. Eur Phys J E 2003;12:111.
[70] Massa MV, Dalnoki-Veress K. Phys Ver Lett 2004;92:255509.
[71] Taden A, Landfester K. Macromolecules 2003;36:4037.
[72] Barham PJ, Jarvis DA, Keller A. J Polym Sci Polym Phys 1982;20:1733.
[73] Cormia RL, Price FP, Turnbull D. J Chem Phys 1962;37:1333.
[74] Baitoul M, Saint-Guirons H, Xans P, Monge Ph. Eur Polym J 1981;17:1281.
[75] Koutsky JA, Walton AG, Baer E. J Appl Phys 1967;38:1832.
[76] McCrum NG, Read BE, Williams G. Anelastic and dielectric effects in polymeric solids. New York: Dover Publications, Inc; 1967.
[77] Yamamoto K, Kato K, Sugino Y, Hara S, Miwa Y, Sakaguchi M, et al. Macromolecules 2005;38:4737.
[78] Pyda M. ATHAS data bank http:web.utk.edu/~athas/databank/1994.
[79] Cho TY, Heck B, Strobl G. Colloid Polym Sci 2004;282:825.
[80] Lu L, Alamo RG, Mandelkern L. Macromolecules 1994;27:6571.
[81] Lorenzo AT, Arnal ML, Müller AJ, Boschetti de Fierro A, Abetz V, submitted for publication.
[82] Douzinas K, Cohen R. Macromolecules 1992;25:5030.
[83] Loo YL, Register RA, Adamson DH. Macromolecules 2000;33:8361.